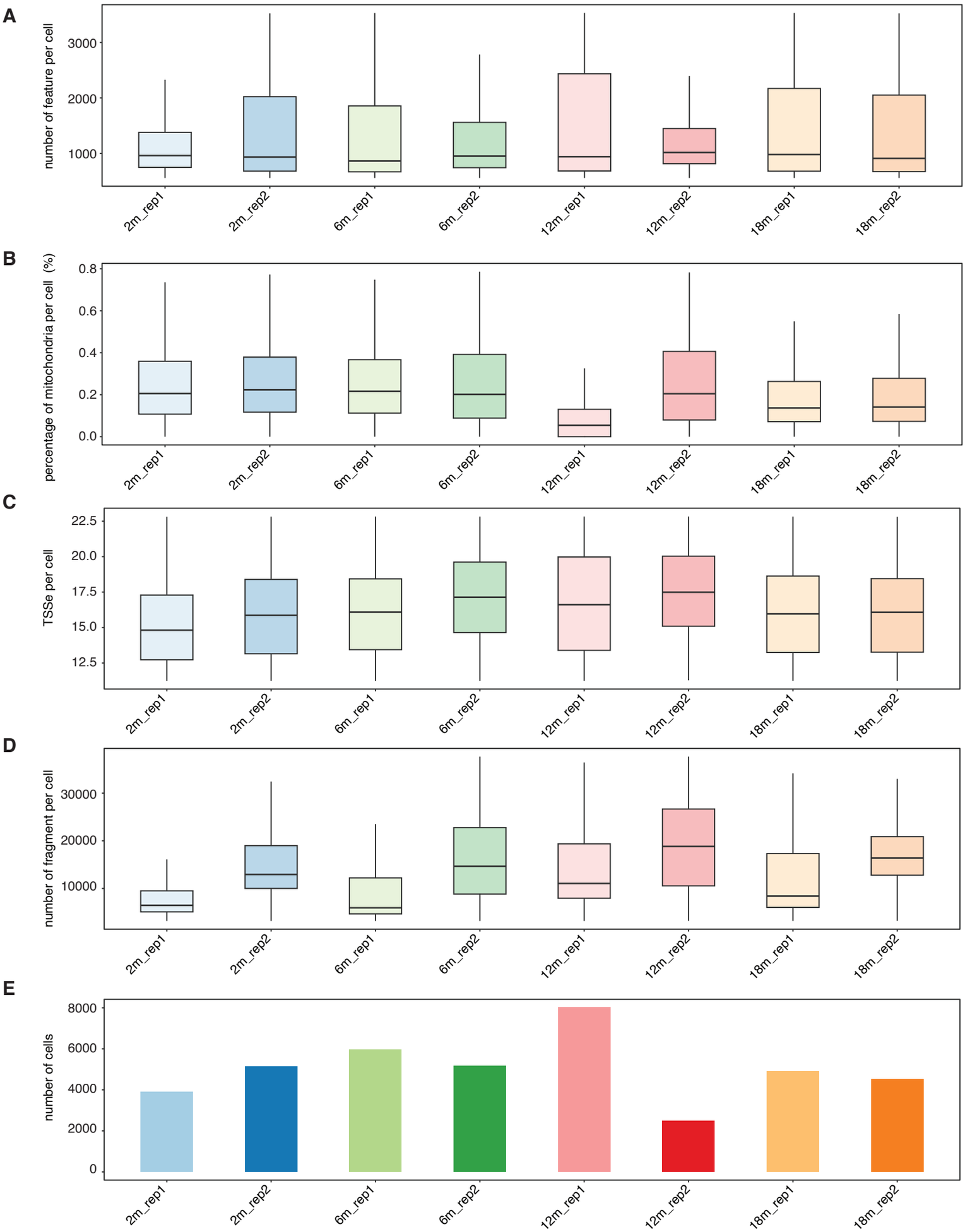

Supplemental Fig. S1: Quality control metrics of the single-nucleus multiome datasets. A, Box plots showing the number of features per nucleus for the RNA modality across samples analyzed in this study. **B,** Percentage of mitochondria reads per nucleus in the RNA libraries from the mouse substantia nigra. **C,** Distribution of transcription start site (TSS) enrichment score for the ATAC modality. **D,** Number of uniquely mapped fragments per nucleus across individual samples. **E,** Bar plots showing the number of nuclei passing quality control for each sample. In panels **A-D**, the boxes span the first to third quartiles, the horizontal line denotes the median, and the whiskers show 1.5x the interquartile range.

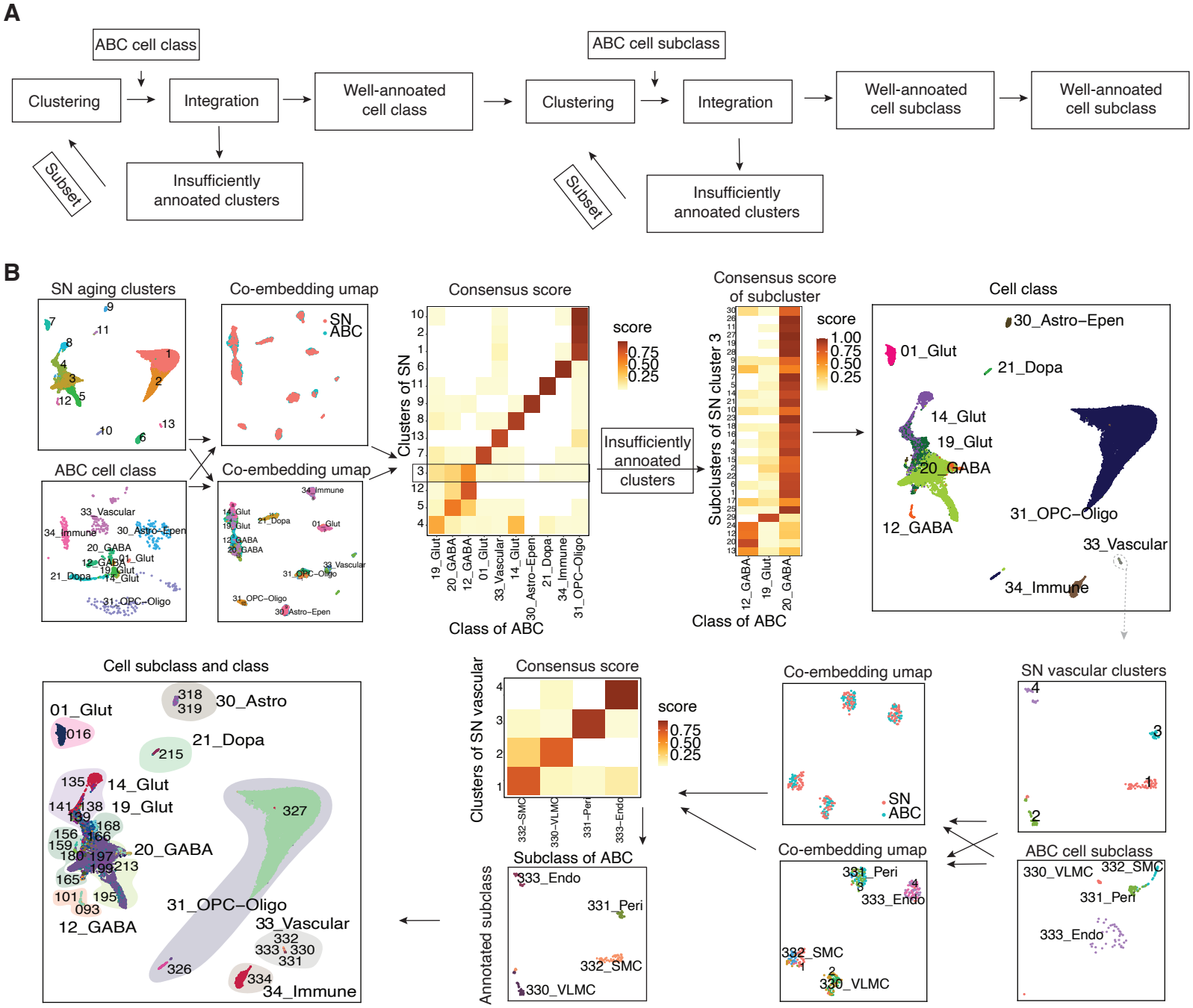

Supplemental Fig. S2: Iterative clustering and data integration for the substantia nigra aging samples. **A,** Overview of the multi-stage cell clustering and integration pipeline applied to all nuclei that passed quality control. **B,** Schematic of the clustering and integration workflow. SN, substantia nigra; ABC, Allen Brain Cell Atlas.

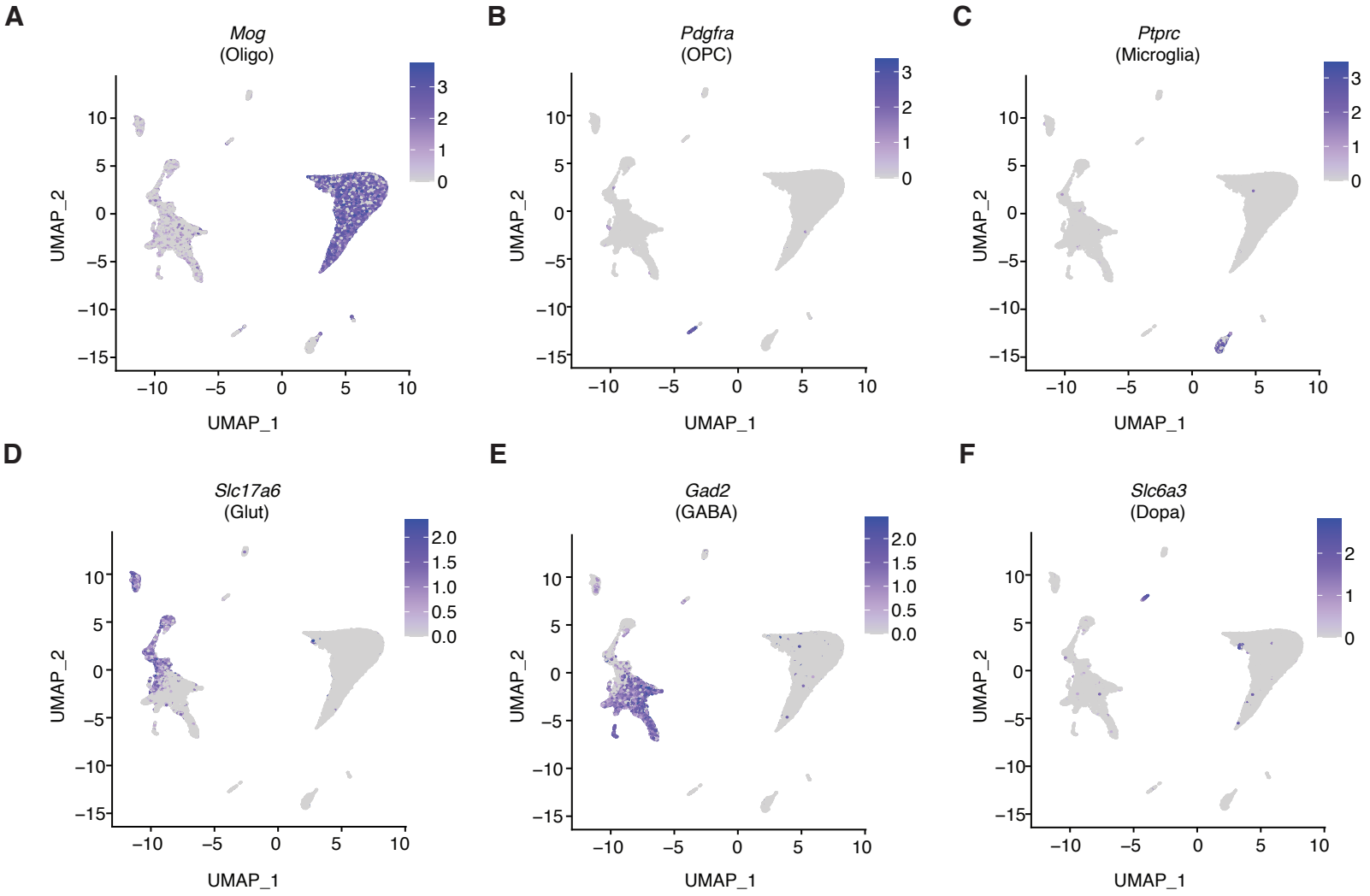

Supplemental Fig. S3: UMAP plots showing expression of representative marker genes. Dots are colored by the normalized gene expression levels of *Mog* (**A**), *Pdgfra* (**B**), *Ptprc* (**C**), *Slc17a6* (**D**), *Gad2* (**E**), and *Slc6a3* (**F**).

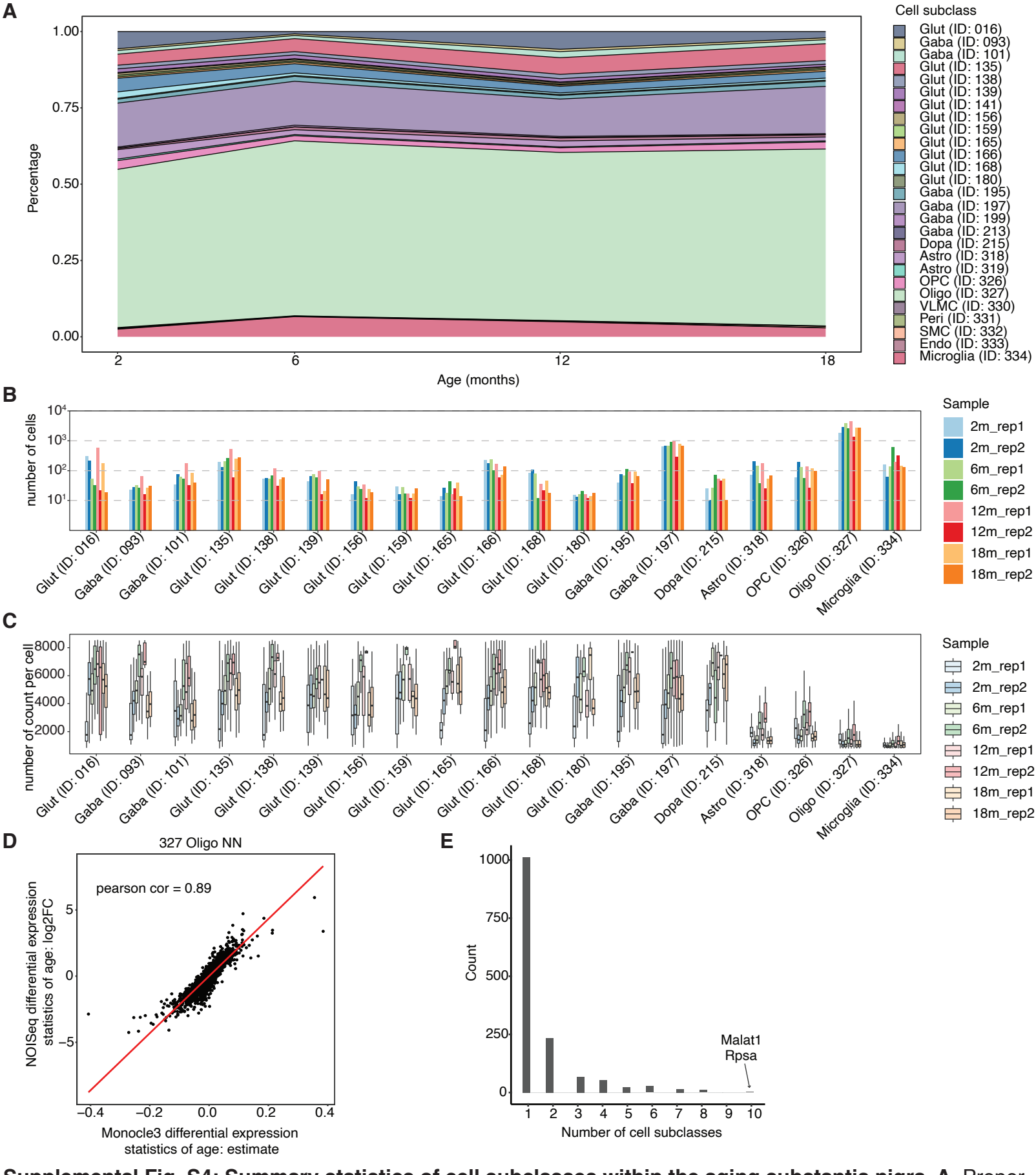

Supplemental Fig. S4: Summary statistics of cell subclasses within the aging substantia nigra. A, Proportion changes of cell subclasses across aging. **B,** Bar plots showing the number of nuclei in each sample across the identified cell subclasses. **C,** Box plots showing the read counts per nucleus for each sample across identified cell subclasses. The boxes span the first to third quartiles, the horizontal line denotes the median, and the whiskers show 1.5x the interquartile range. **D,** Scatter plot comparing $\log_2$(fold change) values from the NOISeq pseudo-bulk analysis with age effect sizes estimated by Monocle3 for the oligodendrocyte subclass. **E,** Histogram showing the distribution of the number of cell subclasses in which each age-associated DEG is significantly detected.

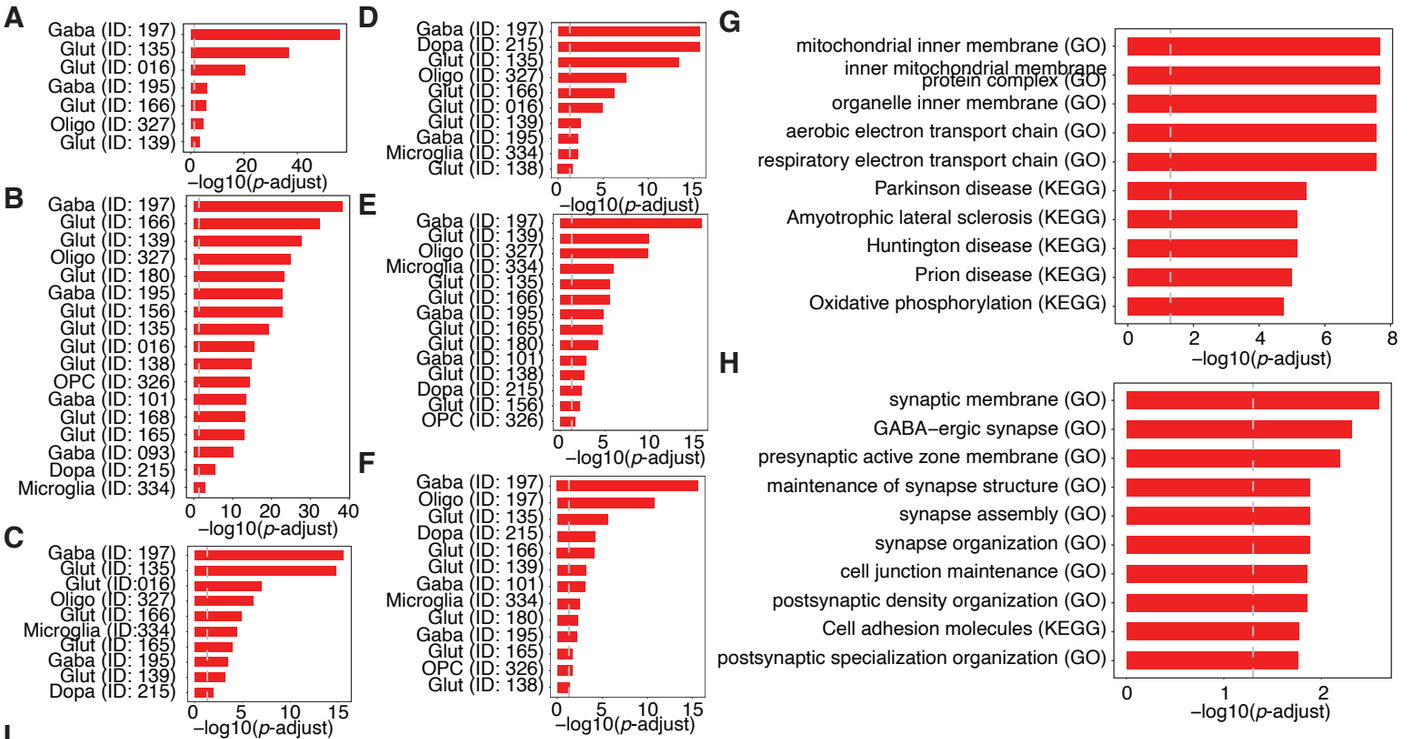

Supplemental Fig. S5: Pathway analysis of age-associated differential gene expression. A, Bar plots showing enrichment of age-associated DEGs in PD KEGG pathway across 7 cell subclasses identified using the Monocle3 model. **B,** Enrichment of age-associated DEGs in PD KEGG pathway across 17 cell subclasses identified using the NOISeq model. **C,** Bar plots showing enrichment of age-associated DEGs in PD-associated genes from MalaCards across 10 cell subclasses identified using the Monocle3 model. **D,** Bar plots showing enrichment of age-associated DEGs in PD-associated genes from Gene4PD across 10 cell subclasses identified using the Monocle3 model. **E,** Bar plots showing enrichment of age-associated DEGs in PD-associated genes from MalaCards across 14 cell subclasses identified using the NOISeq model. **F,** Bar plots showing enrichment of age-associated DEGs in PD-associated genes from Gene4PD across 13 cell subclasses identified using the NOISeq model. **G,** Top enriched GO terms and KEGG pathways for upregulated DEGs during aging identified in dopaminergic neurons using the NOISeq model. **H,** Top enriched GO terms and KEGG pathways for downregulated DEGs during aging identified in dopaminergic neurons using the NOISeq model. The grey dashed line in **A-H** indicates the significance cutoff (FDR < 0.05). **I,** Visualization of the PD KEGG pathway enriched for DEGs upregulated at late aging stages in oligodendrocytes. Age-associated DEGs contributing to this enrichment are highlighted with red boxes.

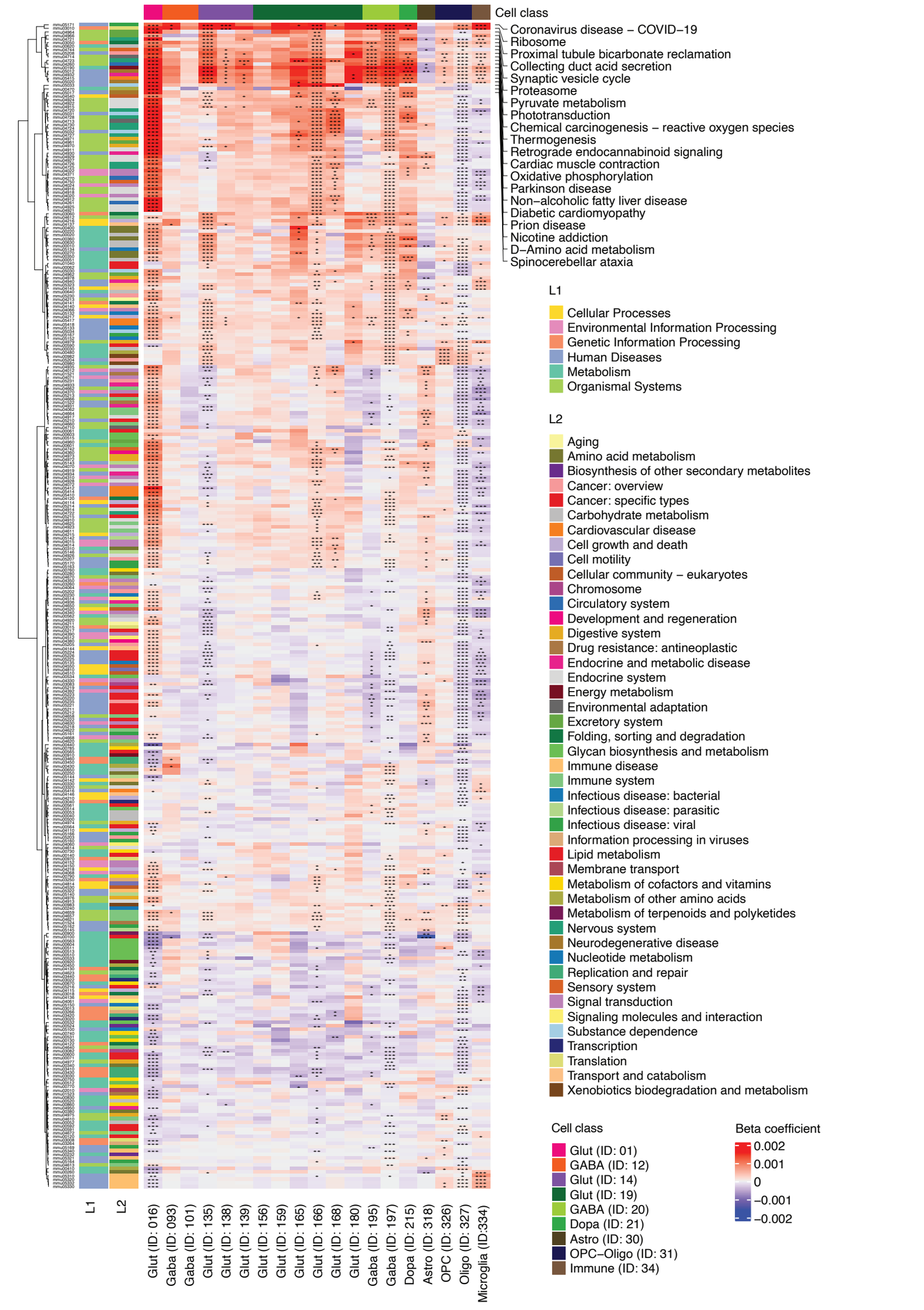

Supplemental Fig. S6: Heatmap showing age-associated differential expression in KEGG pathways. *P*-values were corrected using the Benjamini-Hochberg method for multiple tests. *, FDR < 0.05; **, FDR < 0.01; ***, FDR < 0.001. L1, Level 1 KEGG pathways; L2, Level 2 KEGG pathways.

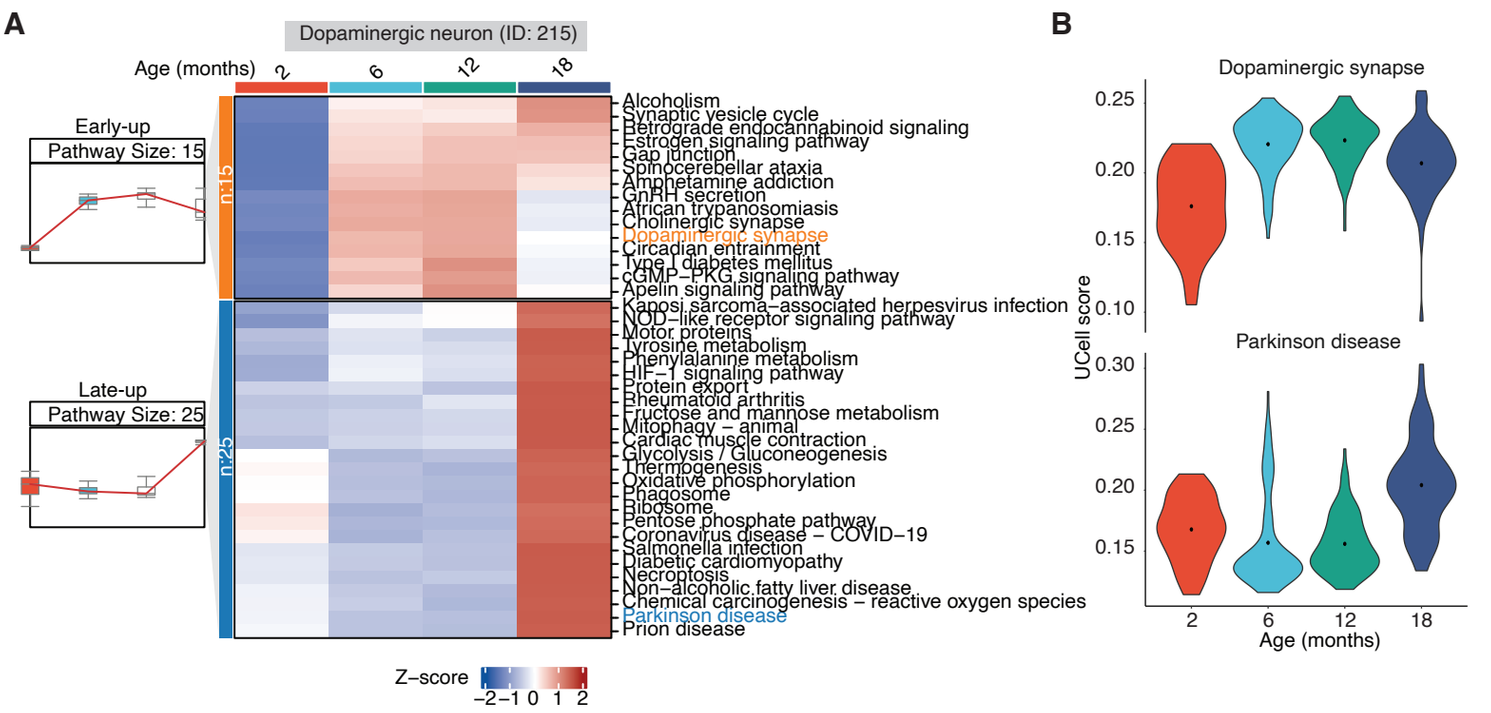

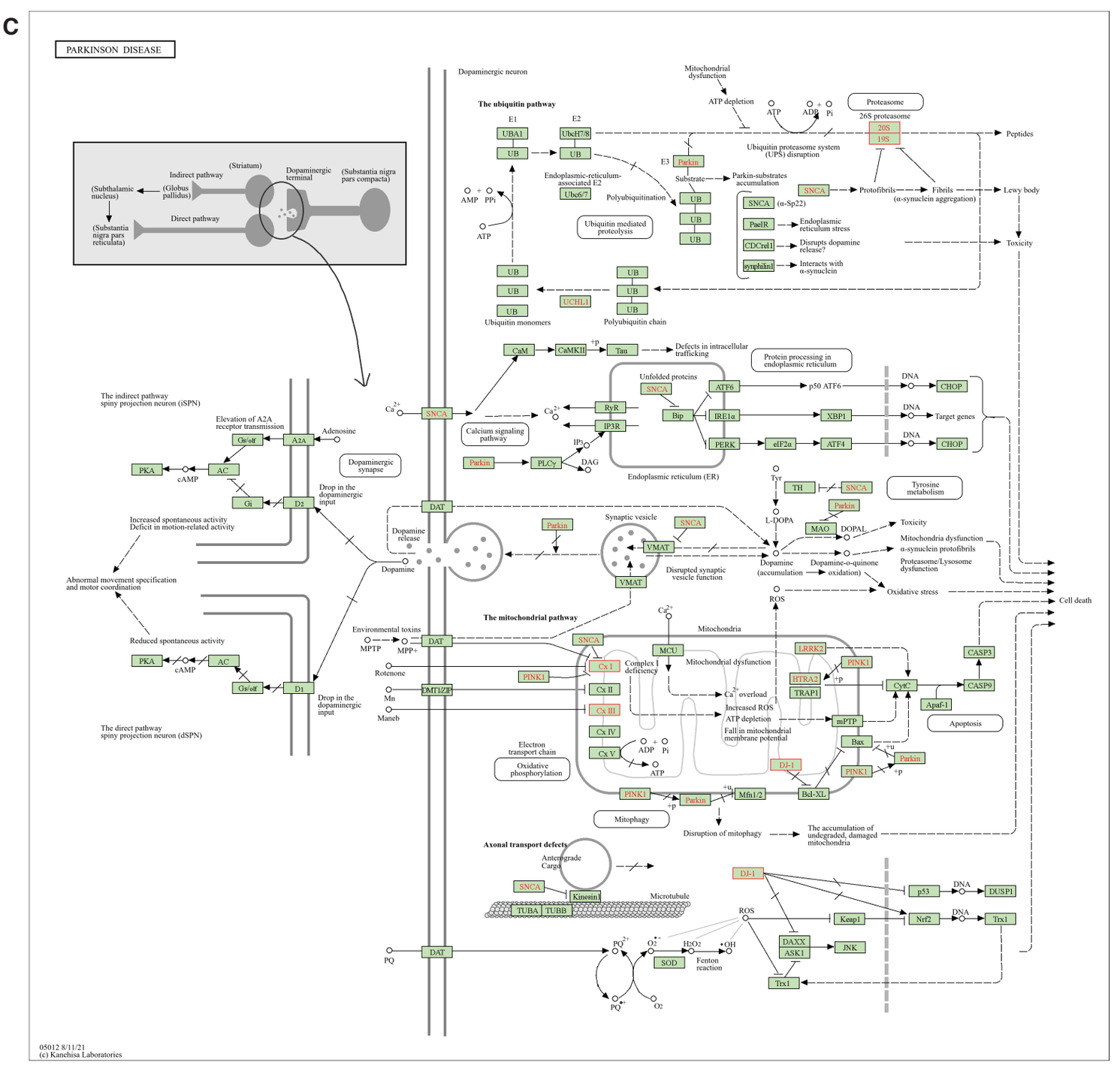

Supplemental Fig. S7: Enriched pathway of age-associated differential gene expression in dopaminergic neurons. A, Groups of age-associated pathways in dopaminergic neurons. Left: Box plots representing UCell scores across ages for two differentially expressed pathway groups. Right: Heatmap of average UCell scores for each pathway group across ages. Early-up, early upregulated pathways in aging; Late-up, late upregulated pathways in aging. **B,** Ucell score distribution of all nuclei in dopaminergic neurons across ages for representative pathways from the two age-associated pathway groups in panel **A**. **C,** Visualization of the PD KEGG pathway enriched for DEGs upregulated at late aging stages in dopaminergic neurons. Age-associated DEGs contributing to this enrichment are highlighted with red boxes.

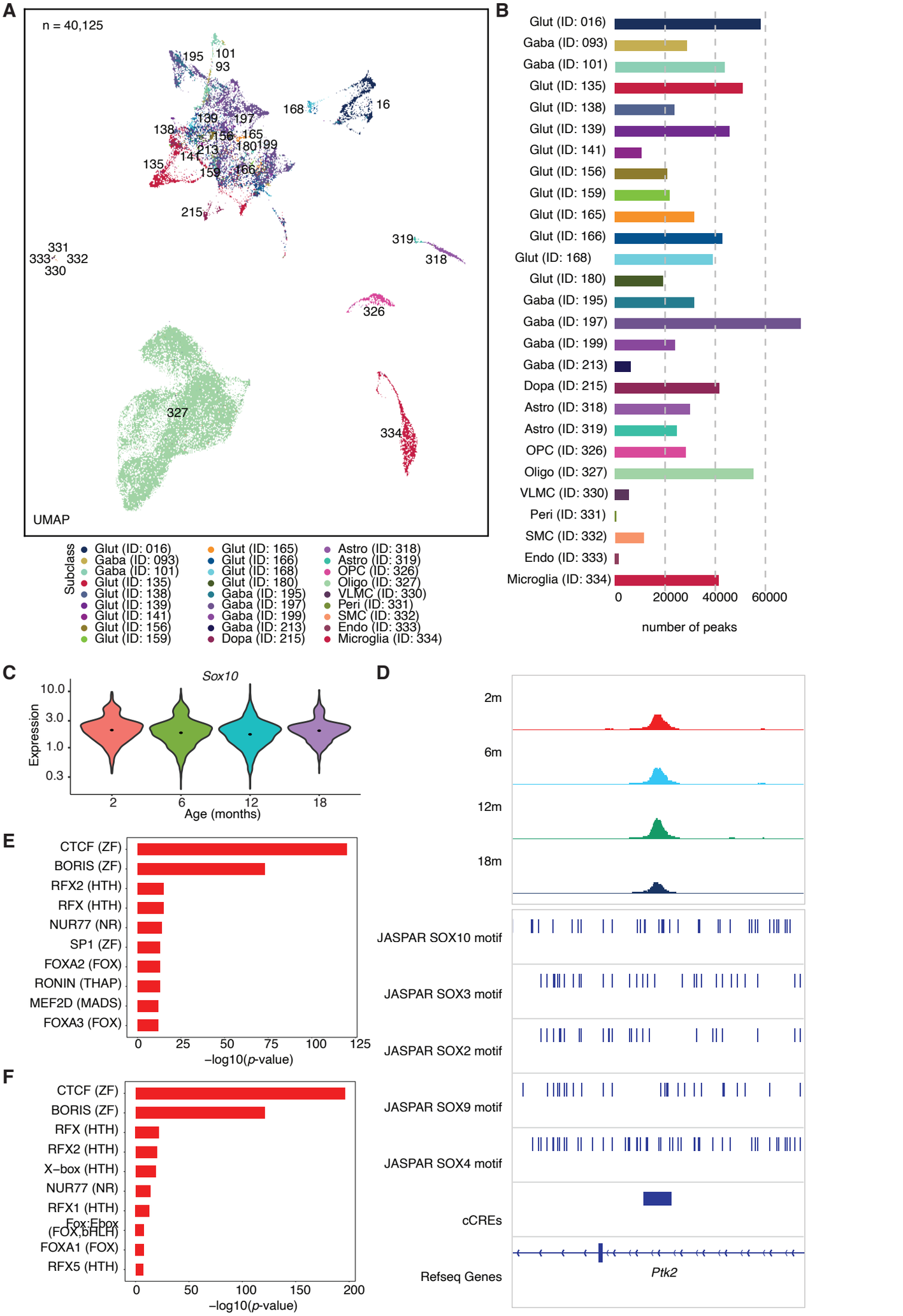

Supplemental Fig. S8: Profiling of chromatin accessibility across cell subclasses in the mouse substantia nigra. A, UMAP embedding of snATAC–seq data (n = 40,125 nuclei). Cells are colored by cell subclass. **B,** Summary of the number of cCREs identified for each cell subclass. **C,** Expression distribution of all nuclei in the oligodendrocytes subclass across ages for *Sox10* gene. **D,** Genome browser tracks showing aggregate chromatin accessibility profiles for the oligodendrocyte subclass across different ages at a representative DAC locus. Predicated motifs from the SOX family (JASPAR database) are show at the bottom. **E,** Bar plots showing top motif enrichment for upregulated DACs in aging identified in dopaminergic neurons using the NOISeq model. **F,** Bar plots showing top motif enrichment for downregulated DACs in aging identified in dopaminergic neurons using the NOISeq model.

A

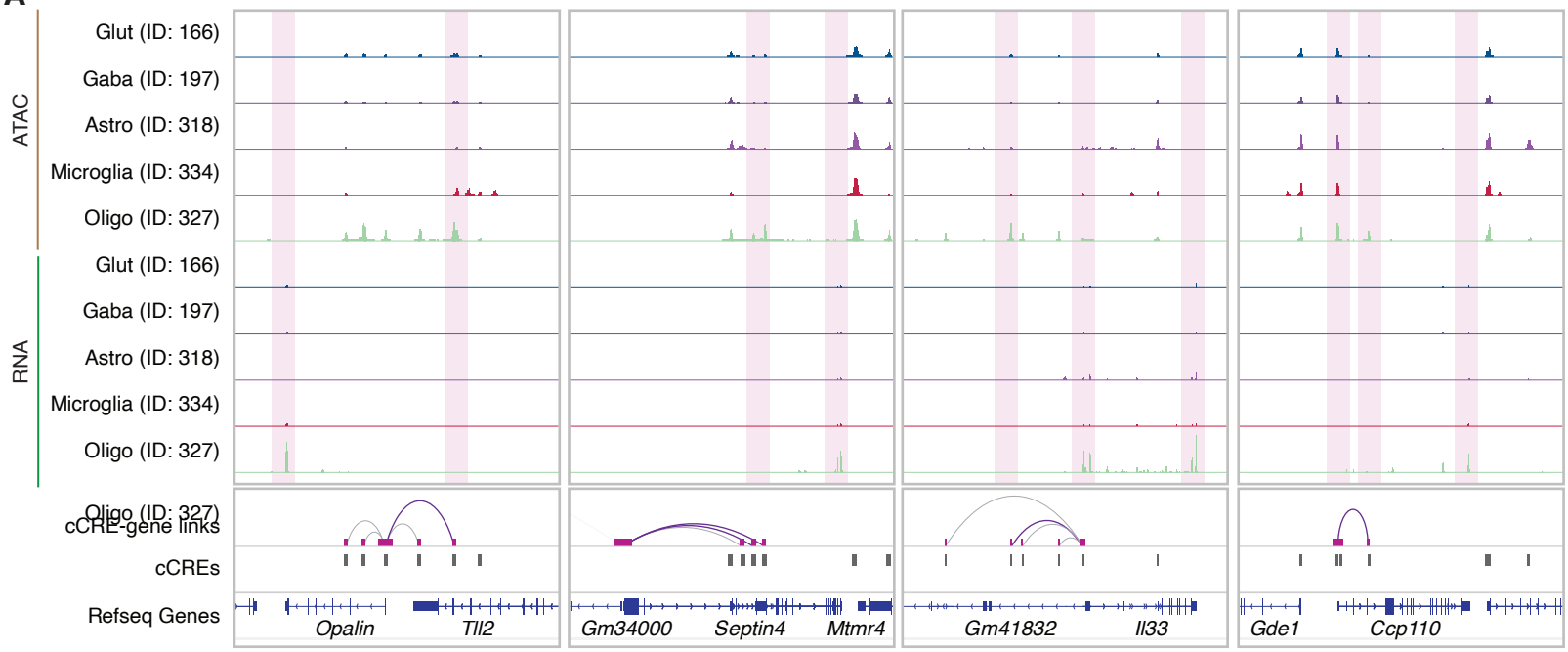

B

Motif	Motif name	Motif family	*P*-value	*Q*-value (Benjamini)	% of Targets Sequences with Motif	% of Background Sequences with Motif
	CTCF	ZF	1e-23	0.0000	40.00%	4.03%
	BORIS	ZF	1e-21	0.0000	43.75%	6.02%
	TCF3	HMG	1e-3	0.0206	16.25%	4.92%
	PRDM15	ZF	1e-3	0.0296	43.75%	25.38%

Supplemental Fig. S9: Analysis of cCREs–gene links in the oligodendrocyte subclass of the mouse substantia nigra. A, Genome browser tracks showing aggregate chromatin accessibility profiles and RNA signals for representative subclasses at selected age-associated DAC and DEG pairs. **B,** Enrichment analysis of motifs within cCREs linked to genes involved in the activated neuroinflammation pathways during aging in microglia. The unadjusted *p*-values were calculated using two-sided Fisher's exact tests.

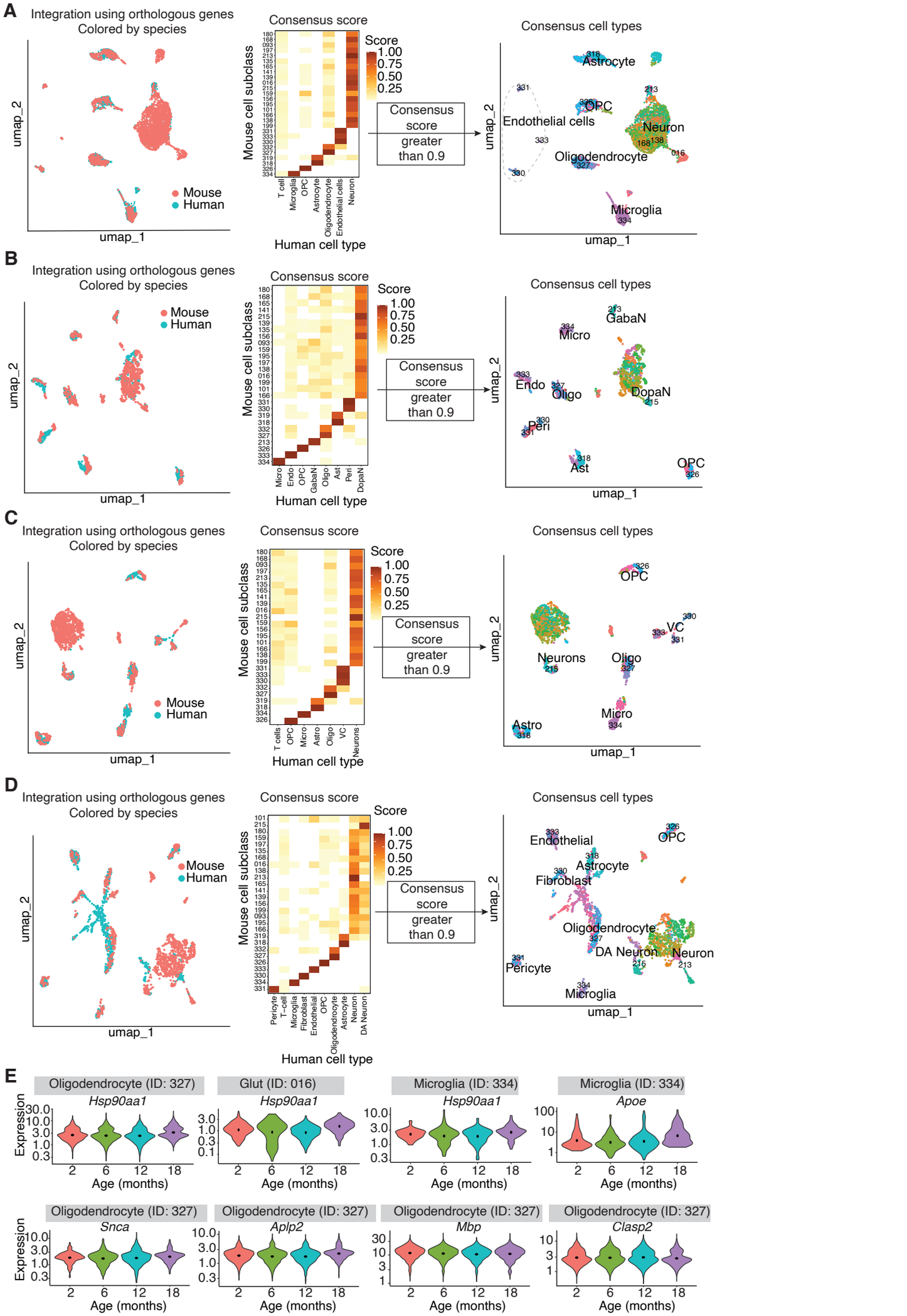

Supplemental Fig. S10: Changes in gene expression during aging related to PD-associated genes. Integration analysis between mouse and human single-cell datasets from Adams et al.(Adams et al. 2024) (**A**), Lee et al.(Lee et al. 2023) (**B**), Martirosyan et al.(Martirosyan et al. 2024) (**C**), and Wang et al.(Wang et al. 2024) (**D**). Micro, microglia; Endo, endothelial cells; GabaN, GABAergic neuron; Oligo, oligodendrocyte; Ast, astrocyte; Peri, pericyte; DopaN, dopaminergic neuron; VC, vascular cells; DA, dopaminergic. **E,** Expression distribution of all nuclei in the consensus subclasses across ages for representative age-associated DEGs related to PD-associated DEGs.

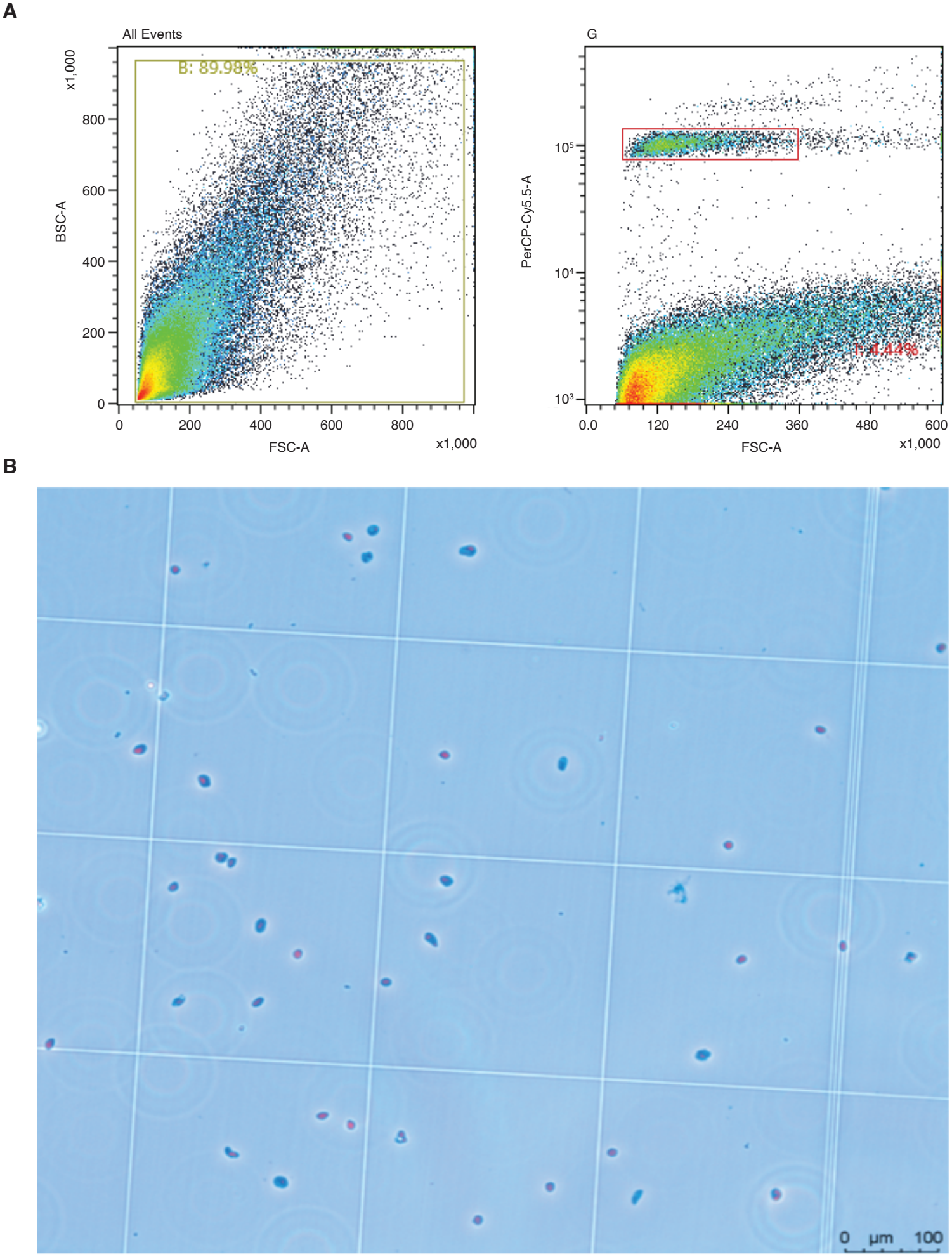

Supplemental Fig. S11: Nuclei gating strategy. A, Nuclei were pooled and stained with Peridinin chlorophyll protein-Cyanine5.5 (PerCP-Cyanine5.5) dye. Potential nuclei were initially identified using forward scatter (FSC) area and back scatter (BSC) area (left dot plot), and subsequently sorted for further analysis (right dot plot). **B,** The nuclei were further validated and counted under a microscope.

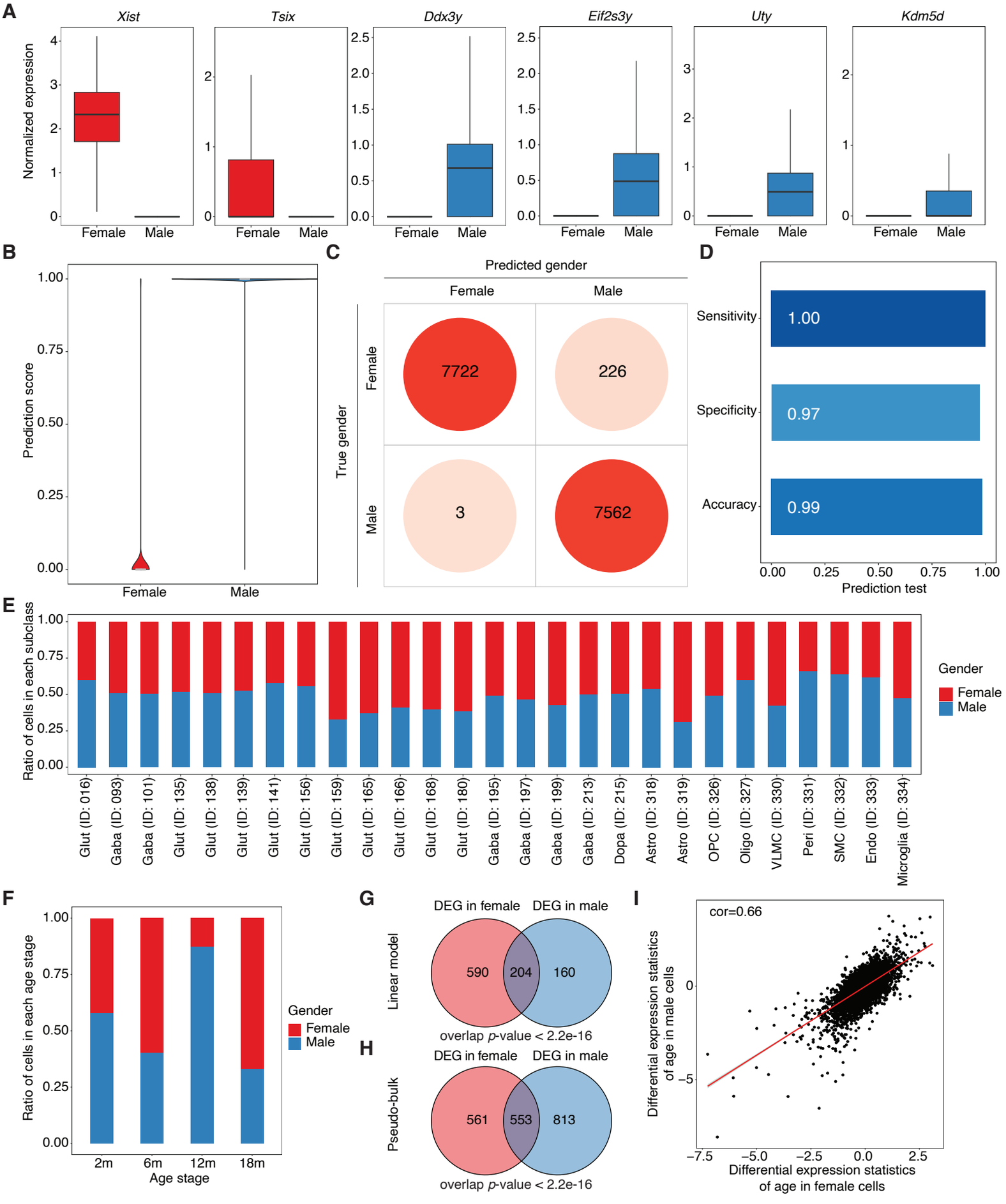

Supplemental Fig. S12: Gender comparison in the SN aging dataset. A, Distribution of normalized expression of six key genes (*Xist*, *Tsix*, *Ddx3y*, *Eif2s3y*, *Uty*, and *Kdm5d*) used for gender prediction model training, separated by gender in the training dataset. **B,** Distribution of prediction scores for gender in the test dataset. **C,** Comparison between predicted gender and true gender in the test dataset. **D,** Bar plot showing the accuracy specificity, and sensitivity of the gender prediction model in the test dataset. **E,** Bar plot showing the proportion of predicted gender cells in each subclass. **F,** Proportion of predicted gender cells across different age stages. **G,** Comparison of age-associated DEGs identified using a linear model for different genders in oligodendrocytes. **H,** Comparison of age-associated DEGs identified using the pseudo-bulk method for different genders in oligodendrocytes. **I,** Scatterplot showing the correlation of age-associated differential expression statistics between male and female oligodendrocytes.

Supplemental Fig. S13: Required number of cells per condition to achieve 80% power under FDR = 0.05 across a range of effect sizes, based on empirical parameter estimates from the oligodendrocyte dataset.

References

Adams L, Song MK, Yuen S, Tanaka Y, Kim YS. 2024. A single-nuclei paired multiomic analysis of the human midbrain reveals age- and Parkinson's disease-associated glial changes. *Nature Aging* **4**.

Lee AJ, Kim C, Park S, Joo J, Choi B, Yang D, Jun K, Eom J, Lee SJ, Chung SJ et al. 2023. Characterization of altered molecular mechanisms in Parkinson?s disease through cell type-resolved multiomics analyses. *Science advances* **9**.

Martirosyan A, Ansari R, Pestana F, Hebestreit K, Gasparyan H, Aleksanyan R, Hnatova S, Poovathingal S, Marneffe C, Thal DR et al. 2024. Unravelling cell type-specific responses to Parkinson's Disease at single cell resolution. *Mol Neurodegener* **19**.

Wang Q, Wang MH, Choi I, Sarrafha L, Liang MRN, Ho LP, Farrell K, Beaumont KG, Sebra R, De Sanctis C et al. 2024. Molecular profiling of human substantia nigra identifies diverse neuron types associated with vulnerability in Parkinson's disease. *Science advances* **10**.